Limnol. Oceanogr., 53(5, part 2), 2008, 2123–2136

Assessing plankton and other particles in situ with the SOLOPC

D. M. Checkley Jr.[1] *and R. E. Davis*
Scripps Institution of Oceanography, La Jolla, California 92093

A. W. Herman
Bedford Institute of Oceanography, Department of Fisheries & Oceans, 1 Challenger Drive, Dartmouth, Nova Scotia B2Y 4A2, Canada

G. A. Jackson
Department of Oceanography, Texas A&M University, College Station, Texas 77845

B. Beanlands
Bedford Institute of Oceanography, Department of Fisheries & Oceans, 1 Challenger Drive, Dartmouth, Nova Scotia B2Y 4A2, Canada

L. A. Regier
Scripps Institution of Oceanography, La Jolla, California 92093

Abstract

We combined a Sounding Oceanographic Lagrangian Observer float with a Laser Optical Plankton Counter (LOPC) and a fluorometer to make an autonomous biological profiler, the SOLOPC. The instrument senses plankton and other particles over a size range of 100 μm to 1 cm in profiles to 300 m in depth and sends data ashore via satellite. Objects sensed by the LOPC include aggregates and zooplankton, the larger of which can be distinguished from one another by their transparency. We hypothesized that the diel production of particles and their loss by sinking and grazing are reflected in the change of the particle distribution. We present data from four deployments of the SOLOPC off California. Particle volume was maximal at the base of the surface mixed layer and correlated with chlorophyll *a* fluorescence. In a 3-d deployment in 2005, particle volume was greatest in the early evening and smallest in the morning, and average particle size increased with depth. Eigenvector analysis of the particle volume distribution as a function of diameter for each of the deployments yielded size peaks characteristic of planktonic crustaceans. Ship-based measurements showed that the abundance of opaque particles of 1.1–1.7 mm equivalent spherical diameter was positively correlated with copepods of this size and simultaneously collected in nets. This relationship was used with SOLOPC data to estimate the distribution of large copepods, which were most abundant beneath the depth of maximal particle flux, estimated from particle size and published sinking rates. Our data are consistent with a model with diel production of particles and their loss by sinking and grazing.

Plankton and other particles are key elements of marine ecosystems and biogeochemical cycles. The euphotic zone is dynamic, with highly variable rates of production and loss of particulate organic matter. New primary production and its export from the euphotic zone are mediated by processes that include mixing, migration, grazing, aggregation, and sinking. Significant variation of these processes occurs on the scale of hours (e.g., diel), days (e.g., events), months (e.g., seasons), and longer and in the vertical (e.g., layers) and horizontal (e.g., across fronts and between water masses). A challenge in oceanography is to measure features of assemblages of particles and plankton with sufficient accuracy, resolution, and regularity to describe their variation and understand their dynamics. We report here on our use of the SOLOPC, an autonomous, Lagrangian profiling float with a conductivity–temperature–depth instrument (CTD), optical particle counter, and fluorometer, to assess plankton and other particles in the upper 100 m off Southern California. Our results are consistent with the diel production of particles, by aggregation of phytoplankton, feces, and detrital material, and their loss by sinking and grazing.

There is a clear need for measurements of plankton and other particles using autonomous, Lagrangian platforms and sensors, or ALPS (e.g., floats, gliders, and autonomous

[1] Corresponding author (dcheckley@ucsd.edu).

Acknowledgments

We thank Jesse Powell (Scripps Institution of Oceanography) and George States (Bedford Institute of Oceanography) for assistance at sea, computer programming, and logistical support; Peter Davison for assistance at sea and computer programming; Lionel Guidi for assistance at sea; and Nadine Eisenkolb for assistance with microscopic analysis of the zooplankton. We thank the captains and crews of the R/Vs *Robert Gordon Sproul* and *New Horizon*. Two anonymous reviewers and Guest Editor Tom Dickey provided constructive comments.

D.C., R.D., and A.H. were supported by National Science Foundation (NSF) grant OCE03-21167. G.J. was supported by NSF grants OCE-0320739 and OCE-0352127.

underwater vehicles with sensors). Ship-based sampling is constrained by the number of research vessels, the cost associated with using them, and the conditions under which they operate. ALPS, by contrast, are far less costly and can be broadly distributed, enabling needed sampling resolution and extent. The Argo program (Roemmich et al. 2004) to measure hydrography exemplifies this new capability. Needed, however, are ALPS with biological sensors. The SOLOPC is such an instrument.

We consider plankton and other particles with an equivalent spherical diameter (*ESD*) of 100 μm to 1 cm, the detection range of the Laser Optical Plankton Counter (LOPC; Herman et al. 2004). Optical plankton counters, including the LOPC, have been successfully used to estimate the abundance of zooplankton, particularly copepods (e.g., Herman 1988; Osgood and Checkley 1997; Heath et al. 1999; Baumgartner 2003; Herman and Harvey 2006). A major challenge has been distinguishing between plankton and other particles in nature (cf., Eppley et al. 1977, for the phytoplankton and particulate organic matter retained on filters). Plankton in the size range we consider includes crustacea (e.g., copepods and euphausiids) and gelatinous taxa (e.g., medusae, tunicates, and eggs and larvae). Other particles present in this size range and found in situ include aggregates, abandoned houses of larvaceans, mucous webs of pteropods, and associated material, living and dead. Many of these 'other particles' are fragile and are not retained by meshes, be they filters or nets (González-Quirós and Checkley 2006). In situ, nondestructive sampling is needed to study such particles.

Multiple ship-deployed optical instruments were used to characterize the in situ particle assemblage in Monterey Bay (Jackson et al. 1997). The volumetric concentration of particles (mL m^{-3}) in this assemblage displayed a broad peak from ~1 μm to ~1 mm *ESD*. Because *ESD* (cf., conserved diameter of Jackson et al. [1997]) is a product of physical size and transparency, opaque objects will have similar *ESD* and physical size, while transparent particles will have a physical size greater than their *ESD*. Particle abundance also varied with depth (Jackson et al. 1997). A moored camera documented diel, episodic, and seasonal variation in particle abundance at 270 m in the northeast Atlantic (Lampitt et al. 1993). Alternative methods to study particles involve filtering, either in situ or in the laboratory. While these methods provide samples of particles for further (e.g., chemical) analysis, they rarely allow for inference about individual particles, particularly in the natural environment, afforded by optical methods.

Plankton, primarily zooplankton, in the size range we consider here has conventionally been studied using meshes, including filters and towed nets. These methods collect physically robust individuals but undersample more fragile taxa, including pelagic coelenterates and tunicates, and do not retain fragile particles, such as aggregates. In situ optical instruments include the Video Plankton Recorder (Davis et al. 1992), Underwater Video Profiler (Gorsky et al. 2000), SIPPER (Samson et al. 2001), and the LOPC. The first three instruments create high-resolution (e.g., 10–100-μm), two-dimensional images that can then be processed using image analysis. The LOPC senses particles that occlude light from laser LEDs sensed by matched 1 mm × 1 mm photodiodes. The relatively large size, power, and data output of in situ video have to date precluded its use in ALPS. Conversely, the relatively smaller size, power, and data of the LOPC allow its use on the Sounding Oceanographic Lagrangian Observer (SOLO) float. However, while video often has sufficient resolution to allow for the identification of plankton and other particles, the LOPC has only a limited ability to do so as a result of its 1 mm × 1 mm element size. Thus, a challenge is to infer about particle type from the LOPC.

The SOLOPC is a synthesis of a SOLO float (Davis et al. 2001), LOPC, and an ECO Puck fluorometer (WET Labs). We describe the SOLOPC and present results from four deployments off Southern California. The oceanography of this region is well studied and described (Eppley et al. 1986; Bograd et al. 2003, and references therein). The California Current (CC) flows southward past Point Conception. Upwelling occurs nearshore, as a result of coastal, alongshore winds, primarily at and north of Point Conception, and offshore, as a result of wind-stress curl (Dever 1997; Rykaczewski and Checkley 2008). Flows from the south include the Davidson Current (coastal, surface) and the California Undercurrent (deep, offshore). The CC (salinity < 33.2) and coastal upwelling (salinity > 33.2) are strongest in spring and summer and the Davidson Current (salinity > 33.2) strongest in winter and autumn. Production at all trophic levels is high in this region (Rykaczewski and Checkley 2008). As with the physical environment, there is strong variation of production in space and time, particularly in relation to upwelling, stratification, diel cycles, storms, and seasons. The particle assemblage consists of plankton and other particles in widely varying amounts (cf., Eppley et al. 1977; González-Quirós and Checkley 2006). We hypothesized that diel variation in primary production in the upper water column would result in diel variation in the abundance of particles derived from the phytoplankton, including aggregates (cf., Lampitt et al. 1993; Ruiz 1997). To test this hypothesis, we assessed plankton and other particles hourly for 12 h to 4 d in the upper 100 m during four deployments of the SOLOPC off Southern California.

Methods

SOLOPC—The SOLOPC (Fig. 1) is a combination of the SOLO, LOPC, and ECO Puck fluorometer. The principle of operation of each of the three component instruments is unchanged. The novelty of the SOLOPC lies in the integration of the three components.

The SOLO is the fourth generation of an autonomous float originally described by Davis et al. (1992). The float regulates buoyancy by pumping oil between an external bladder and the interior of the pressure case. Power is generated from internal batteries and communications are by satellite. For use in the SOLOPC, the SOLO was altered to carry the additional mass in water of the LOPC and ECO Puck chlorophyll *a* (Chl *a*) fluorometer, to sink at a sufficient speed for LOPC operation, to power and communicate with the LOPC, and to transmit data to the

Fig. 1. SOLOPC being lowered during deployment. Overall length is 2.5 m; weight, 36 kg (air) and 0 ± 100 g (water). Laser Optical Plankton Counter (LOPC) is bottom left. Circular-tipped antenna is for GPS and Iridium. Argos antenna has red flags. CTD sensors are between antennae. Electrical cable connecting SOLO and LOPC visible above stability disk and over pneumatic bladder. ECO Puck fluorometer not visible, but located below stability disk.

user via the Iridium satellite communications system. The wall thickness of the SOLO pressure case was reduced to lessen its weight in water. A faired adaptor, made of Delrin, was mounted at the base of the SOLO, below the oil-filled bladder, to carry the LOPC. The Plexiglas stability disk was reduced in diameter to lessen drag and thus increase terminal sinking speed. A connector penetrating the pressure case and an electrical cable were added to transmit power and data between the SOLO and LOPC. The lithium battery pack was divided in two equal parts, one to power the SOLO and the other to power the LOPC and ECO Puck fluorometer. An Iridium modem and antenna were added. The SOLO firmware was revised to integrate the SOLO and LOPC, including control commands, data transfer, and Iridium communications. The SOLO contains standard sensors for pressure, temperature, and conductivity, as well as a GPS receiver. Data are processed internally, binned to ~1 m, and presented as a single text file for each ascent. SOLO data are stored in memory, as well as transmitted to the user via Iridium.

The LOPC is the second generation of optical plankton counter originally described by Herman (1988). The LOPC (Herman et al. 2004) uses a narrow (1-mm) laser light beam and a geometrically matched linear diode array as a receiver, thereby reducing the individual sampling area of each diode element to 1 mm × 1 mm. The effective size of the sheet of light is 7 cm × 7 cm, the cross section of the LOPC sample tunnel, through which water with particles flows. Particles are sensed as they pass through this sheet of light. The photodiode output is digitized at 1 MHz and processed by a digital signal processor in real time. The peak, negative-going change in voltage sensed by each diode occluded by a particle is termed the digital size (*DS*). A particle that occludes one or two elements is termed a single element particle (SEP). A particle that occludes three or more elements is termed a multiple element particle (MEP). SEP *DS*s are accumulated over a preset time interval (e.g., 0.5 s for the standard, towed LOPC) and stored as a *DS*-frequency distribution. For each MEP, the start time and duration of occlusion of each diode element and its *DS* are recorded. Thus, the LOPC data stream consists of periodic *DS*-frequency distributions for SEPs and a set of features for each MEP when it is sensed.

The LOPC mass and firmware were altered for use in the SOLOPC. The aluminum sample tunnel was replaced with a lighter one made of black Delrin to reduce mass. The time interval for creating an SEP *DS*-frequency distribution was increased from 0.5 to 3 s to compensate for a flow rate slower than the towed instrument was designed for, to allow ~0.5–1-m depth bins within a profile and to reduce the volume of data to be transmitted via Iridium. All MEP data are retained. The LOPC binary data are compressed and parsed into 1940-byte packets for Short Burst Data (SBD) communication with Iridium. Both compressed and uncompressed binary files are stored in LOPC memory, and SBD files are transferred to the SOLO for Iridium transmission.

An ECO Puck Chl *a* fluorometer (WET Labs) is fastened to the SOLO below its stability disk. An electrical cable between the fluorometer and the LOPC transmits power and data. Analog data from the fluorometer are acquired by the LOPC, digitized, and incorporated into the binary data of the LOPC. We report digital values of Chl *a* fluorescence.

The flow of power, data, and commands for the SOLOPC while it is deployed and operating autonomously are shown in Fig. 2. Prior to deployment, the SOLO is attached to an external computer. A magnetic switch is used to turn on power to the SOLO. Memory is purged, diagnostic tests are performed, and mission parameters are set. The SOLOPC is disconnected from the external computer and deployed. A shallow (e.g., 40-m) diagnostic dive is made first, and, if this dive is successful, the mission continues. During descent, the SOLO pressure sensor, LOPC, and fluorometer receive power and acquire data and store it in memory. At a preset (“turn-off”) depth (e.g., 100 or 150 m), data acquisition by the LOPC and fluorometer is stopped, the LOPC transfers data to the SOLO, and the SOLOPC decelerates. After LOPC data transfer to SOLO is complete, the LOPC is turned off.

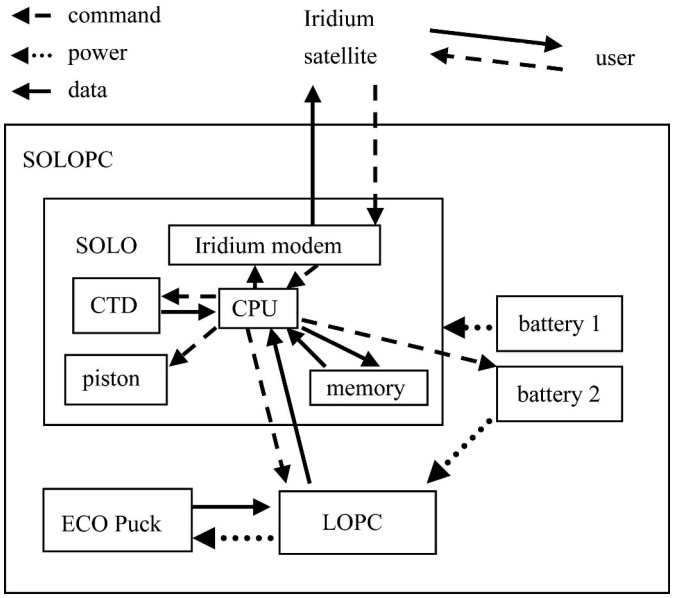

Fig. 2. Flow diagram showing power, data, and control of SOLOPC.

During ascent, the LOPC and fluorometer remain off and the CTD on, and data are acquired and stored in memory. Upon reaching the surface, the CTD is turned off, the pneumatic bladder of the SOLO is inflated, a GPS position is acquired, and communication to Iridium is established. Data are transferred to and commands received from the user via Iridium. Once communications are complete, a new dive begins. If recovery is intended, the mission is commanded to end, the float remains at the surface, periodically transmits a GPS position, and is located and retrieved. In the laboratory, the SOLO once again is attached to a computer, powered, data in its memory downloaded, and it is turned off. The LOPC is powered from an external supply, the data are downloaded to an attached computer, and then it is turned off.

Ship-based sampling—A plankton net with LOPC and CTD inside was used to simultaneously obtain a sample of plankton, for microscopic analysis, and LOPC data, for comparison. This net consists of a 0.5-m–diameter, 78-μm mesh net with filtering cod end. An LOPC is mounted inside the net such that the entrance to the sample tunnel (standard 7 cm $\times$ 7 cm cross section) is flush with the bridle ring. The ratio of areas of the net to LOPC is 40. A CTD is mounted behind the LOPC. The CTD is powered via and transmits data to the LOPC. On one cruise (Sproul 2005), a WETStar (WET Labs) Chl *a* fluorometer was also mounted in the net; this was powered from the ship and data were acquired by the LOPC. The 'net-LOPC' was hauled vertically with an electromechanical cable, enabling power and data transfer between the lab and instruments, from 100 m to the surface at 1 m s^{-1}. The net was rinsed and the plankton sample preserved in a buffered solution of 5% formalin : seawater. On one cruise (Sproul 2007) the net without electronics was used, as described above.

Analysis of zooplankton samples—Ashore, in the laboratory, net collections from each cruise were analyzed to provide data to compare with those from the LOPC. Sample identities were masked and samples randomized prior to analysis. Copepods larger than ~1 mm cephalothoracic length (CL) were enumerated for comparison with data from the LOPC. These included *Metridia pacifica* adults, *Calanus pacificus* copepodite stage 5 (C5) and adults, *Pleuromamma borealis* adults, and all other copepods with CL as large as or greater than that of *M. pacifica* adult females. We termed this group large copepods (LCs). All LCs in all or a known fraction of each plankton sample were counted, until at least 30 *C. pacificus* adult females were enumerated. The concentration of LCs was estimated from the number of individuals of that type in a sample divided by the net mouth area times the tow depth.

Data analysis and presentation—Binary files from the LOPC, acquired from either the SOLOPC (via Iridium or from memory) or the towed LOPC (real time) were converted to text files using commercial software (Brooke Ocean Technology). Data files from the towed LOPC contained simultaneously acquired temperature, salinity, and pressure data from the attached CTD and, on one cruise (Sproul 2005), Chl *a* fluorescence. For the SOLOPC, LOPC, Chl *a* fluorescence, and pressure data were acquired on each descent and were associated with temperature, salinity, and pressure data acquired during the subsequent ascent. We term these data a single dive. For graphic presentation of property distributions of SOLOPC data, we calculated values of temperature, salinity, sigma-*t*, Chl *a* fluorescence, and particle abundance for 1- or 5-m bins over 5–100 m of each dive.

Particle size: We now describe how we calculate a single size spectrum from data for SEPs and MEPs. We define the *ESD* as the value assigned to a particle of any shape, the volume of which is equivalent to the volume of an opaque sphere of that diameter. We define the occluded diameter (*OD*) as the number of 1-mm elements a particle attenuates, either partially or entirely. Thus, $OD > ESD$ for a translucent particle, whereas $OD \sim ESD$ for an opaque particle. The size of SEPs and MEPs is expressed as *ESD*. The LOPC was calibrated by the manufacturer (Brooke Ocean Technology) by recording the *DS* for an SEP, or the sum of the *DS*s (ΣDS) for the elements occluded by an MEP, for opaque spheres ~100 μm–1 cm in diameter. For SEPs, these data were used to create a look-up table resident in the LOPC microprocessors. For MEPs, calibration bead diameter was regressed on ΣDS:

$$ESD = 0.1806059 + 2.54589 \times 10^{-4}\Sigma DS - 1.0988 \times 10^{-9}\Sigma DS^2 + 9.54 \times 10^{-15}\Sigma DS^3 \quad (1)$$

For an environmental particle, *ESD* for an SEP is estimated from *DS* and the look-up table, and for an MEP it is estimated from ΣDS and Eq. 1. Shape is not used because the calibration has been completed with opaque spheres and our desire is to have measurements of SEPs and MEPs that are comparable. In essence, the same

principles of measurement are used to estimate *ESD* for SEPs and MEPs. A single *ESD* frequency distribution for all particles in a single time or depth interval was created by combining *ESD* values of SEPs and MEPs in that interval. The conserved volume (sensu Jackson et al. 1997) of particles was calculated using *ESD* and assuming a sphere. The volume concentration of particles (dimensionless) is expressed in mL m^{-3}, equivalent to parts per million (volume : volume; cf., Jackson et al. 1997).

Attenuance index and LC abundance: For each MEP, we computed an attenuance index:

$$AI = \text{mean}(DS_{MEP}) \,/\, DS_{MAX} \quad (2)$$

where DS_{MAX} is the maximal *DS* (i.e., complete occlusion of a diode element) and mean(DS_{MEP}) is the mean *DS* for the MEP. *AI* varies over the range of 0 (transparent) to 1 (opaque). We classified MEPs sensed by the LOPC as possible LCs by using $AI > 0.6$ and $1.1 < ESD < 1.7$ mm (i.e., relatively opaque MEPs in the size range of LCs from microscopic measurement of LCs in our plankton samples and published *ESD* values; Osgood and Checkley 1997; Beaulieu et al. 1999).

Normalized particle volume spectra: We express the abundance of particles as a function of their size using the normalized particle volume spectrum (Jackson et al. 1997). An alternate expression, not used here, is the normalized biomass size spectrum (e.g., Herman and Harvey 2006). All MEPs were assigned an *ESD* as above. Particle counts within a depth range of 5 m were collected into the appropriate logarithmic size bands, with the ratio of upper to lower *ESD* for each band equal to 1.1447. The sample volume for the depth range was calculated by multiplying cross-sectional area of the LOPC tunnel (49 cm^2) by the SOLOPC sinking velocity and time interval for the depth range. The particle number spectrum $n_{i,j}$ for the *i*th band and *j*th depth range was calculated by dividing the number of particles within each band by the sample volume and the *ESD* range for the band (Δd_i). The volume spectrum *nV* was calculated by multiplying n_{ij} by $\pi d_i^3/6$, the volume of a particle with an *ESD* equal to median *ESD* for the band, d_i. The normalized volume spectrum was calculated as *nVd*. The volume spectrum is normalized so that the area under the curve is proportional to integrated particle volume when plotted against the log of *ESD*. The resulting spectra for the New Horizon cruise (see below) spanned *ESD*s from 106 μm to 0.54 cm in 30 bands and were represented as vectors. Each spectrum was matched with the mean Chl *a* fluorescence measured for its profile within its 5-m depth interval.

Particle flux: The particle flux *F* (g dry wt m^{-2} d^{-1}) was calculated by multiplying the mass spectrum *nm* by the particle settling speed v_s and numerically integrating over the spectral (d) size range:

$$F = \int nmv_s \mathrm{d}d \quad (3)$$

where n is the particle number spectrum and m is the dry weight of a particle with diameter d (mm). Particle mass m and v_s were estimated as a function of d using the relationships of Alldredge and Gotschalk (1988):

$$m = 8.8d^{1.125} \quad (4)$$

$$v_s = 50d \quad (5)$$

Eigenvectors for normalized particle volume spectra: Each *nVd* spectrum describes the average particle volume distribution for a fixed depth interval, usually 5 m, during one dive. It is represented as a vector at the standard diameters used to calculate n. The vector was trimmed to eliminate those diameters for which all measured values were 0. The spectrum of mean values of *nVd* was calculated for each cruise and subtracted from individual spectra before calculating eigenvectors. The covariance matrix from the resulting accumulation of *nVd* vectors was used to determine eigenvectors. These were sorted in order of decreasing eigenvalues. That is, the first eigenvector explains the largest fraction of the *nVd* variance. Eigenvector analysis is also known as principal component analysis (e.g., Preisendorfer 1988) and empirical orthogonal function analysis (e.g., Emery and Thomson 1997). It is used to decompose a large number of variables, here the normalized volume spectral values at the d_i, into a minimal number of co-varying patterns. Negative values of the eigenvector are possible as a result of the mathematical analysis.

Results

Cruises and SOLOPC deployments—We report on three cruises, with four SOLOPC deployments, off Southern California (Fig. 3). The first (SP05) was on the R/V *Robert Gordon Sproul* in September–October 2005 east of Catalina Island, during which SOLOPC 1, not yet with an ECO Puck fluorometer, made 64 dives. The second cruise (NH06) was on the R/V *New Horizon* in September 2006, southwest of Point Conception, during which SOLOPC 1 made 86 dives. The third cruise (SP07) was on the R/V *R.G. Sproul* west of San Diego, during which SOLOPCs 1 and 2 made 10 and 13 dives, respectively. Twenty-four vertical tows with the net and LOPC were made near the SOLOPC during SP05, and 10 such tows were made near the SOLOPC during NH06; on SP05 a fluorometer was also used. Two net tows, without electronic instruments, were made during SP07.

SOLOPC performance—Terminal sinking speed of the SOLOPC was achieved by approximately 10 m in depth and ranged from 0.20 to 0.25 m s^{-1}, the value depending on the float drag and buoyancy and, in turn, on the maximal float density and seawater temperature and salinity. The nadir of the float trajectory was approximately 1.3–1.9 times the LOPC "turn-off" depth (100 m for the four deployments reported here) and depended on float buoyancy and density structure of the water column. Terminal ascent speed was approximately 0.15 m s^{-1}. The

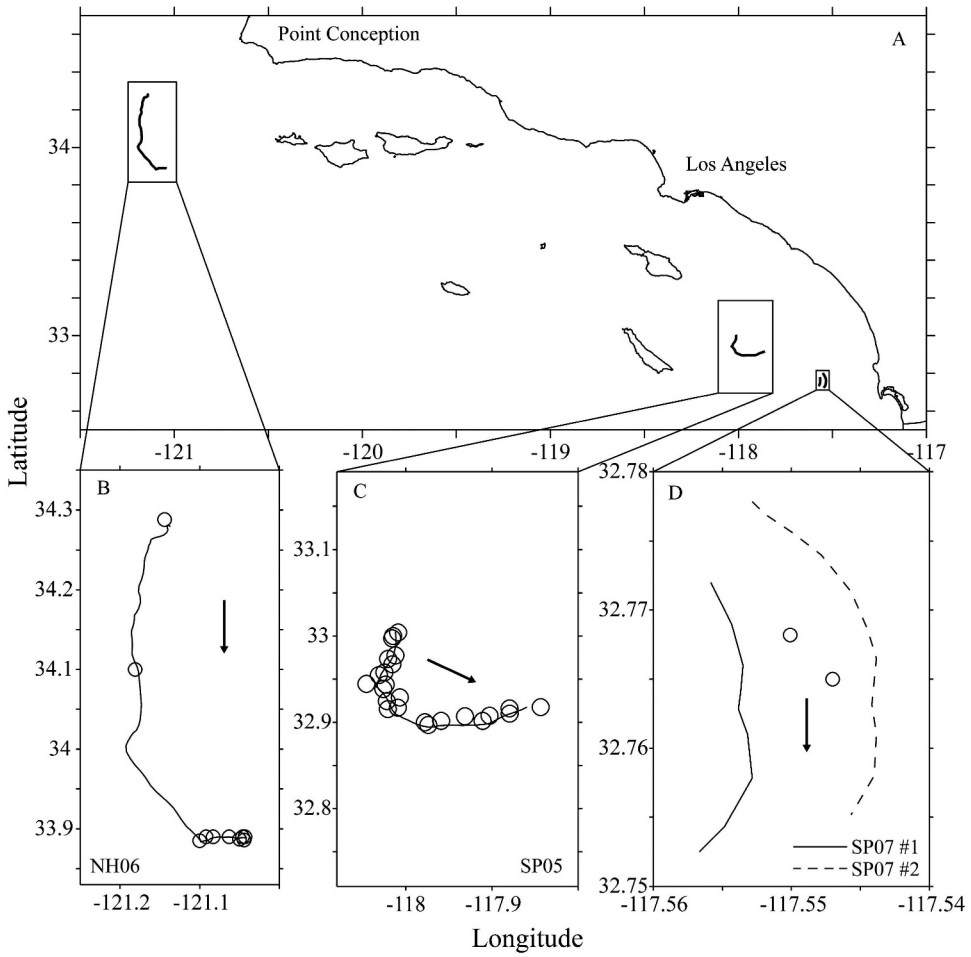

Fig. 3. Map of SOLOPC deployment locations. (A) Southern California Bight; (B) NH06; (C) SP05; and (D) SP07 1 (left) and 2 (right). Lines are trajectories of SOLOPC. Arrows indicate direction of movement. Circles show locations of net-LOPC (B, C) and net (D) tows from ship.

time for a complete dive cycle (with 100-m "turn off" depth), including Iridium communications, was approximately 1 h and varied with particle concentration (hence, amount of data transferred) and sinking and rising speeds. We estimate approximately equal power usage by SOLO, including Iridium communications, and the LOPC and a maximal possible number of dives with 100-m "turn-off" depth to exceed 300.

Sinking speed of the SOLOPC can be accurately estimated from measured pressure and time, and flow through the LOPC tunnel is estimated from the transit time of small particles using an algorithm in the LOPC firmware (Herman et al. 2004). The average of the ratio of the rates of estimated tunnel flow to sinking rate was 0.72–0.93 for the 50–80-m depth stratum.

Property distributions—SP05. The SOLO CTD was mistakenly programmed to turn off earlier than intended during this, the first, deployment of the SOLOPC; hence the lack of near-surface hydrographic data (Fig. 4). A mixed layer extended to 10–18 m, below which the water column remained stratified. There was no apparent long-term trend in the physical properties. Temporal variation on the scale of internal waves, with 12–24-h period, was apparent. The SOLOPC did not have a fluorometer during SP05, but the ship-deployed fluorometer showed a Chl *a* maximum layer at ~20–25 m, immediately beneath the mixed layer. Particles sensed by the LOPC (Fig. 4) were most abundant, both numerically (particles m^{-3}) and by volume (mL m^{-3}), at ~20 m, below the base of the mixed layer. The concentration of particles, by number and volume, was greatest near sunset and least near sunrise (Figs. 4, 5). Total particle volume was more variable and high values were distributed more deeply than those for particle number, indicating that most smaller particles occurred at ~15–35 m, whereas occasional, large-*ESD* particles occurred well below the depth of the Chl *a* maximum. Particle volume, binned into four 6-h periods centered on sunrise, noon, sunset, and midnight (Fig. 5), showed a distinct pattern with time of day and depth. The particle concentration (mL m^{-3}) maximum over the 24-h period was at 15–25-m depth and 0.5–1.0-mm *ESD*. The peak concentration was maximal at sunset and minimal at sunrise. At all times of day, there was an increase in particle size with depth.

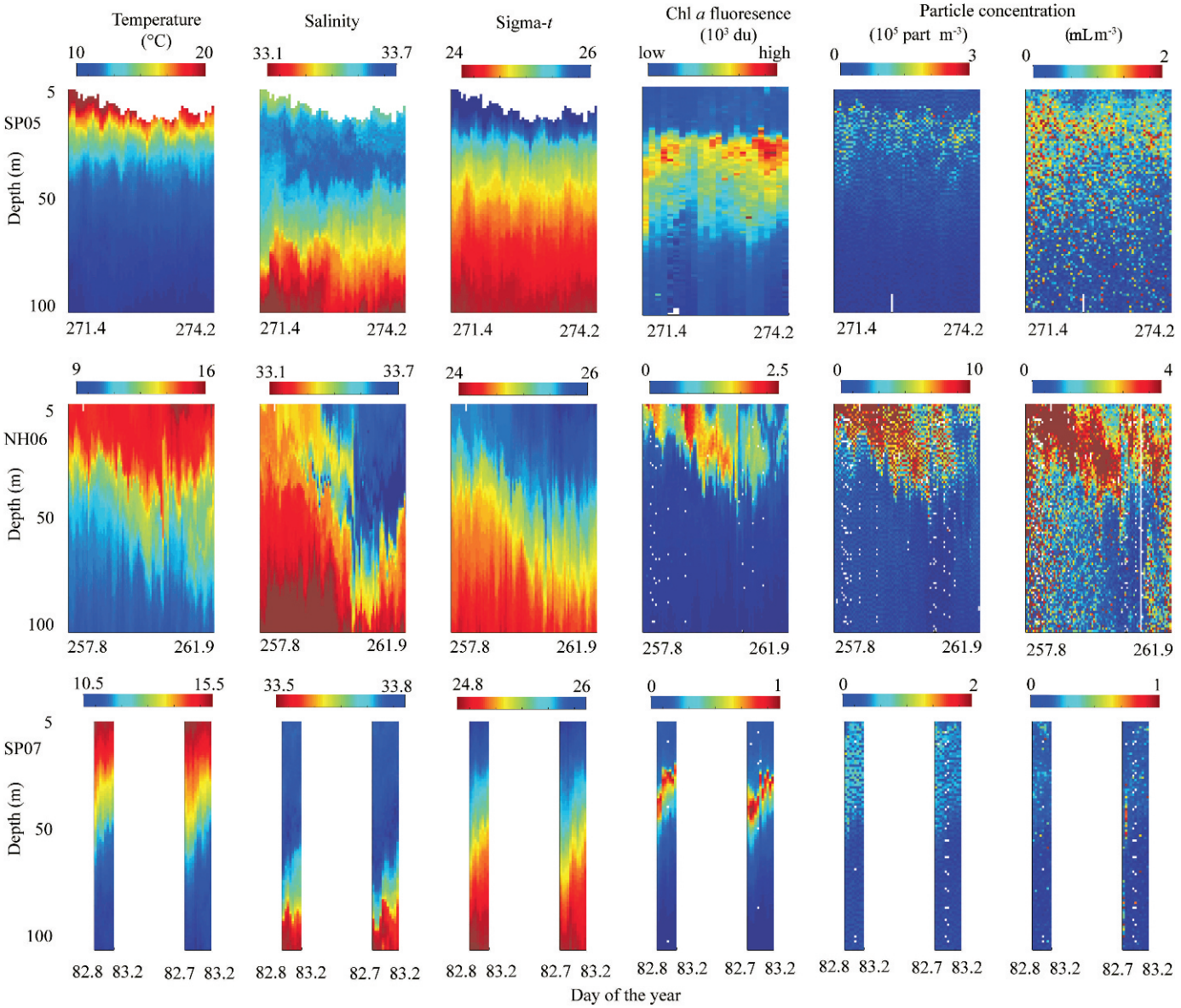

Fig. 4. Property distributions measured by the SOLOPC. From top to bottom: SP05, NH06, and SP07 (SOLOPC 1 to left and SOLOPC 2 to right for each variable, for SP07). Deployment dates (day of year) are shown for start and end of each deployment in 2005 (SP05), 2006 (NH06), and 2007 (SP07). From left to right: temperature, salinity, and sigma-*t*, Chl *a* fluorescence (digital units [du] comparable between deployments for NH06 and SP07), and total particle concentration by number and by volume. SOLOPC in SP05 did not yet have a fluorometer, and Chl *a* fluorescence data are from the fluorometer deployed from the ship in the net-LOPC.

NH06: The water column was stratified during most of this deployment (Fig. 4). Notable was an intrusion of low-salinity (<33.2) water, beginning subsurface (~30 m) on dive 26 and reaching its maximum (surface to 50–80 m) by dive 56. Variation on the scale of 12–24 h was also evident. Chl *a* fluorescence was initially maximal nearest the surface, in the high-salinity water, but the maximum deepened with the intrusion (Fig. 4). Particle concentration (both number and volume) varied similarly, with maximal values near surface initially and deepening mid-deployment. As in SP05, the volume of particles was more variable and broadly distributed with depth than was the number of particles. Diel variation of particle abundance was not as apparent in NH06 as in SP05 as a result of water mass variability.

SP07: These two, brief test deployments were also in a stratified water column. The two SOLOPCs replicated one another well (Fig. 4). Chl *a* fluorescence was maximal in the thermocline and shoaled slightly from evening through morning. Particle concentration, by number and volume, was greatest in and above the Chl *a* fluorescence maximum in terms of numbers and in and below the Chl *a* fluorescence maximum in terms of volume (Fig. 4).

Particles—MEP opacity: Equivalent spherical diameter is calculated from the *OD* and transparency for each MEP. Comparison of *ESD* and *OD* for MEPs provides insight into the characteristics of particles of different sizes. To illustrate this, we plot *ESD* as a function of *OD* for all

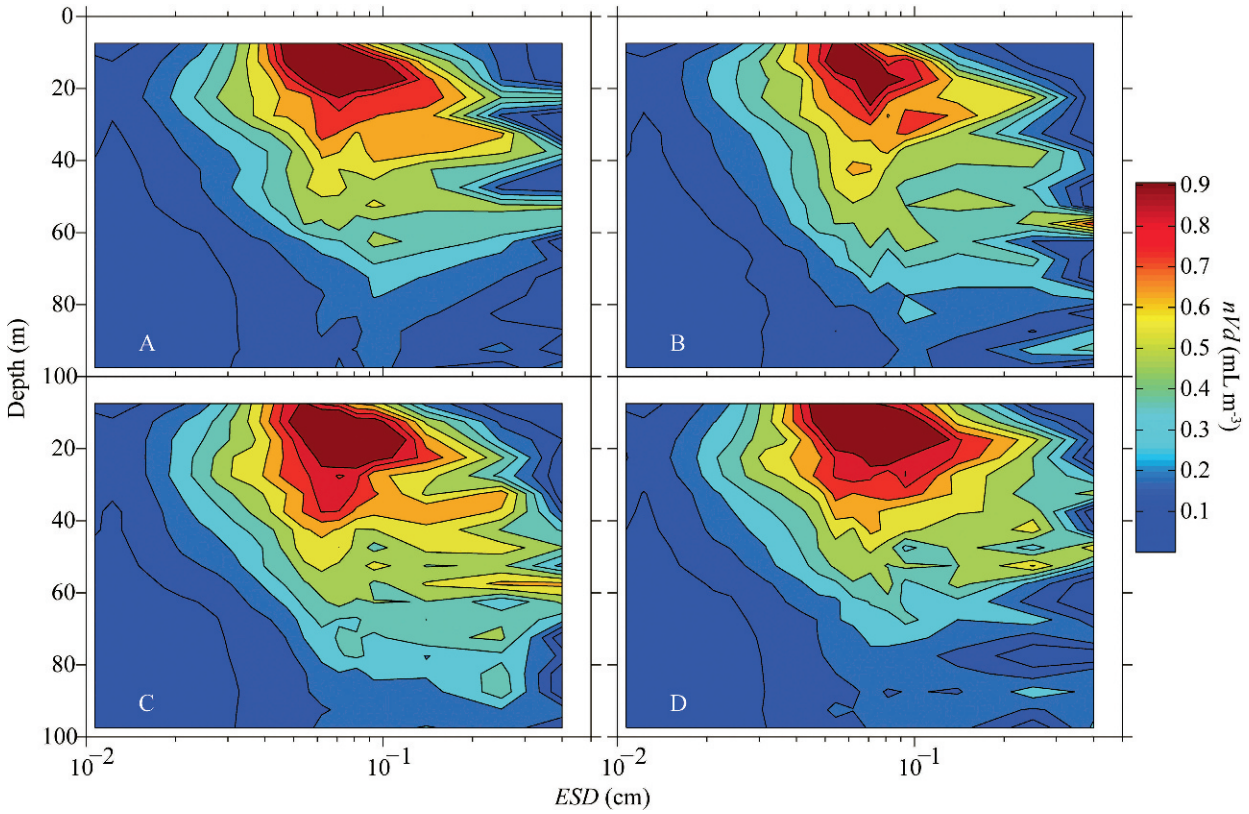

Fig. 5. Daily cycle in particle concentration for SP05. Profiles were averaged in 6-h bands, centered on local noon. If local noon is 12:00 h, the panels represent (A) late night, 21:00–03:00 h, $n = 18$; (B) early morning, 03:00–09:00 h, $n = 12$; (C) midday, 09:00–15:00 h, $n = 18$; and (D) late afternoon, 15:00–21:00 h, $n = 15$.

MEPs in NH06 (Fig. 6). The white line is $ESD = OD$ (i.e., the relation for opaque objects). All values fall below this line. Particles near the white line are of high opacity and have an OD of up to ~1 cm. Particles nearer to the abscissa are of high transparency (low opacity), with some as large as 1.5 cm OD, but each with a far lower ESD (<~1 mm). Similar distributions exist for SP05 and SP07 (not shown).

Eigenvectors: The mean value of nVd as a function of ESD had a Gaussian-type shape (Fig. 7A). The maximal value was about 0.5 mm for the two deployments during Sproul 2007 and about 0.7 mm for the both the Sproul 2005 and New Horizon 2006 cruises. The integrated volume of the mean nVd spectrum was greatest for NH06 and least for SP07 (2.5 and 0.4–0.5 mL m^{-3}, respectively). The fractions of variance in nVd explained by eigenvectors 1 (Fig. 7B) and 2 (Fig. 7C) were 14% and 11% (SP05), 16% and 10% (NH06), 19% and 14% (SP07 1), and 19% and 10% (SP07 2), respectively.

Zooplankton—Estimates of the abundance of LCs based on the analysis of LOPC data (counts m^{-3}) were not different from estimates of these zooplankters based on microscopic analysis of net samples (individuals m^{-3}) (Fig. 8). We used data for 12 net-LOPC tows during SP05 and nine during NH06 that were near the SOLOPC. We assumed a filtration efficiency of the net of 0.75. To estimate LCs from LOPC data, we considered only MEPs with $AI > 0.6$ and 1.1–1.7-mm ESD. The net-LOPC–based estimates of LC abundance explained 72% of the variability in estimates of LC abundance from microscopic analysis of the net samples ($r^2 = 0.72$, $p < 0.01$, $n = 21$; Fig. 8).

Particle flux and zooplankton—Estimated particle flux (Fig. 9) was greatest in the region of highest particle concentration (Figs. 4, 5). Diel variation in particle flux was apparent, particularly in SP05. The abundance of MEPs corresponding to LCs was greatest beneath the depth of maximal flux. The number of such particles counted by the SOLOPC on each dive was small as a result of the small volume (7 cm × 7 cm × 100 m = 0.0049 m^3) sensed, precluding strong inference about diel variation in their abundance and distribution.

Discussion

SOLOPC performance—Deployment and recovery of the SOLOPC are similar to that for the SOLO (i.e., at times challenging, but feasible under most conditions). The appropriate balance of buoyancy and drag enables the SOLOPC to attain a sinking speed minimally acceptable for the LOPC within 5 m of leaving the surface. Sinking rate, once terminal velocity was achieved, was stable. The nadir depth of 1.3–1.9 times the LOPC "turn-off" depth, together with the operational depth limit of the LOPC

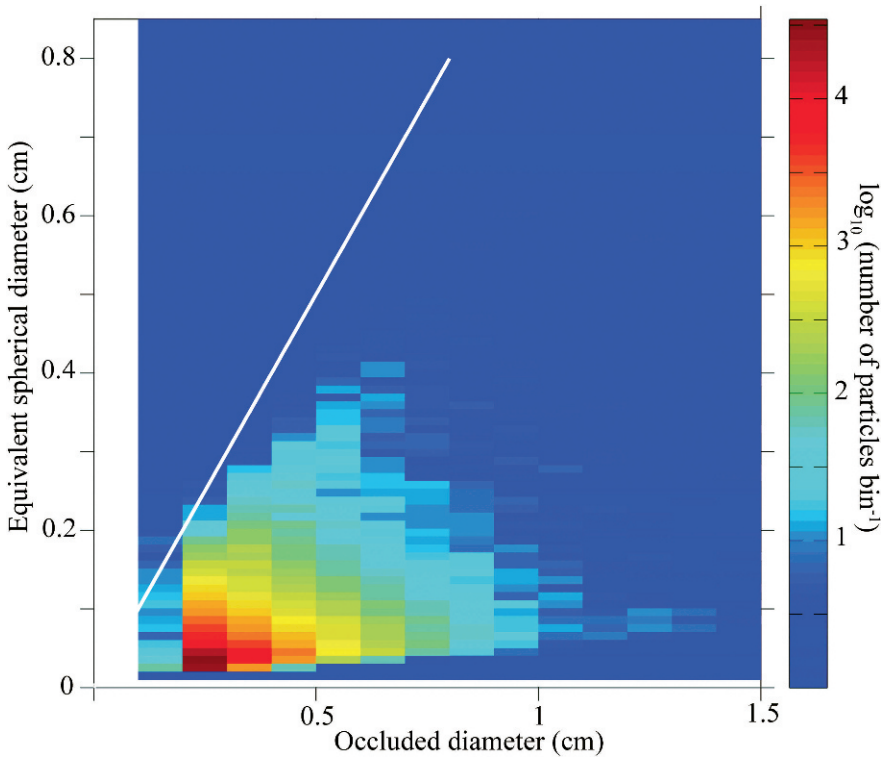

Fig. 6. Distribution of MEP properties for all profiles in NH06. The occluded diameter (*OD*) is the number of light beams attenuated by the object passage times the beam width (1 mm); equivalent spherical diameter (*ESD*) is the diameter calculated from opacity and *OD* (*see* text). Counts were accumulated in bins 0.1-cm wide; the color represents $\log_{10}$ of the number of counts in a bin. The white line is where $OD = ESD$.

(600 m), limit the "turn-off" depth of the SOLOPC to 300–460 m. The SOLOPC can be programmed, before or during a mission, to remain at depth (to 600 m) for a specified time. Short Burst Data Communication with Iridium worked well, even in high sea state. The SOLO and LOPC data transmitted ashore via Iridium exactly matched those downloaded from internal memory in the SOLOPC after recovery.

Sensor fouling is a potential problem we have not yet addressed. Our deployments to date (four reported here, three subsequently in coastal to oceanic locations) have been relatively short (most 3–5 d, 60–100 dives) and have not shown evidence of sensor fouling, as assessed visually. Fouling may be minimized by short deployments and/or 'parking' the SOLOPC at depth between dives. Fouling remains a concern and merits future attention.

The SOLOPC, like the SOLO float, provides valuable data on hydrography and, in addition, on plankton and other particles. An advantage of the SOLOPC is its autonomous operation in a Lagrangian frame of reference, freeing it from ship motion, which can be of the same magnitude as the winch speed for wire-deployed instruments. This mode of deployment, combined with its relatively slow sinking speed, may cause the SOLOPC to be a 'stealth' sampler of zooplankton and other particles. Zooplankton avoidance and the disaggregation of fragile particles with the SOLOPC may be minimal compared to those associated with other types of sampling. Another attribute of the SOLOPC is its ability to profile the euphotic zone at a constant interval of ~1 h, enabling investigation of diel processes, including the dynamics of plankton and other particles, with a temporal resolution and regularity usually not feasible from a ship.

MEP properties—There are diverse types of plankton and other particles sensed by the SOLOPC, ranging from copepods and euphausiids to aggregates and fecal pellets, and combinations of these. The availability of multiple measurements for each MEP allows us to explore the nature of the larger particles. A comparison of *OD* with the *ESD* shows the heterogeneous nature, with regard to transparency, of particles (Fig. 6). If particles were all solid, opaque objects, the *OD* and *ESD* should be approximately the same. While there are such particles (*see* following section), most have an *OD* that is much larger than their *ESD*. Such relatively transparent particles could be aggregates or gelatinous zooplankton. These results are consistent with those of González-Quirós and Checkley (2006) and Herman and Checkley (unpubl.), in which aggregates were found to be as or more abundant than zooplankton.

Zooplankton—Our ability to quantify the zooplankton using data from the LOPC depends on abundance, size, and type of zooplankton in relation to other particles. The *nVd* distribution for *ESD* of <~1 mm is broad and lacks

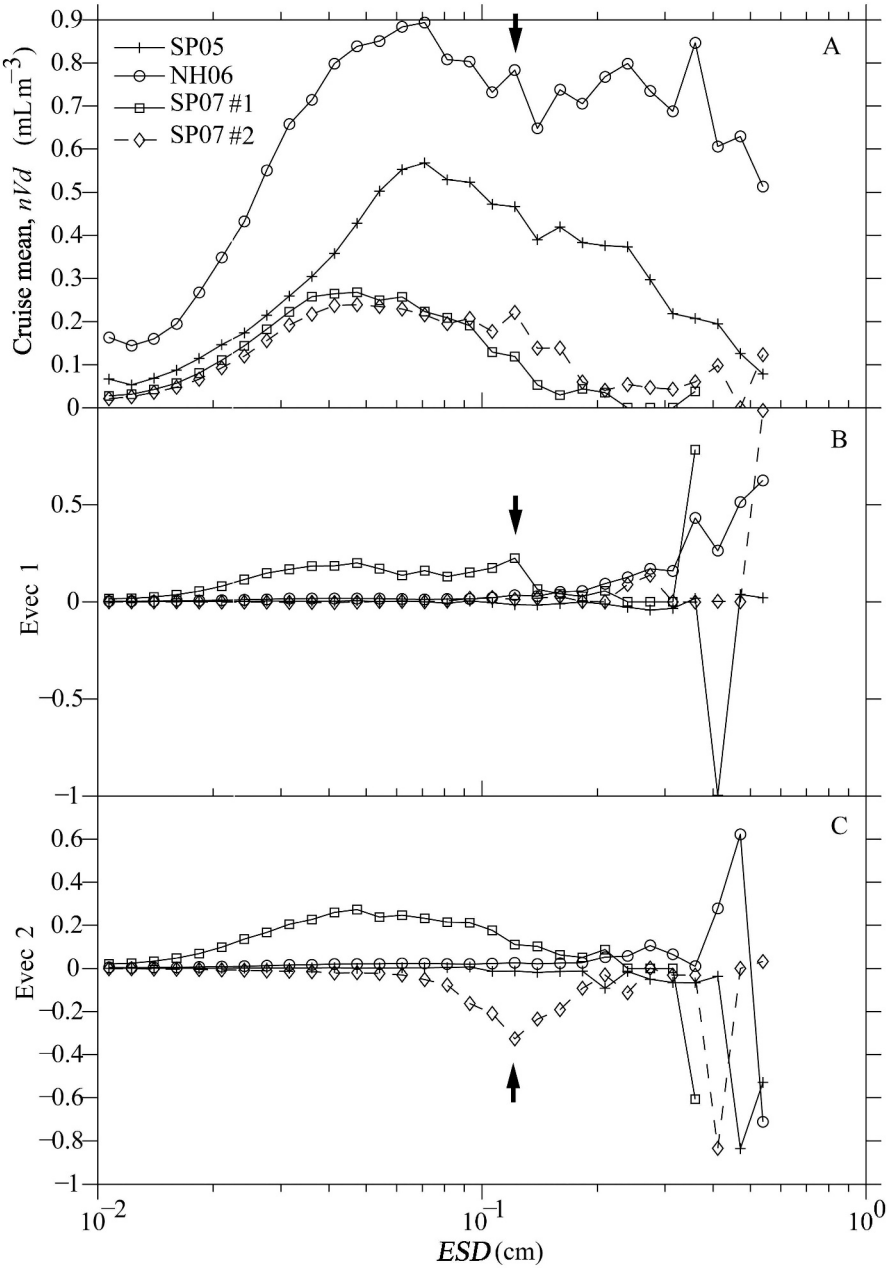

Fig. 7. Particle volume spectrum, nVd (mL m^{-3}), described by the mean and two first eigenvectors (mL m^{-3}) as functions of *ESD*. (A) Mean distribution, (B) first eigenvector (normalized to a length of 1), and (C) second eigenvector (normalized to a length of 1). Shown are the results for the four deployments. Black arrows depict peaks and trough proposed to correspond to *ESD* of *Calanus pacificus* C5 and adults (*see* text).

distinct peaks (Fig. 7). Thus, it is difficult to distinguish discrete size classes of zooplankton from other particles in this size range. The size range of 0.1–1 mm is believed to contain aggregates and other types of particles than plankton (cf., Jackson et al. 1997). Our eigenvector analysis indicates that the spectrum of particles with *ESD* of $>\sim 1$ mm often contains distinct peaks or troughs, consistent with these being due to discrete size classes of zooplankton, including copepods and euphausiids. The abundance of large copepods microscopically counted in net samples and that estimated from the LOPC data, including only relatively opaque particles of 1.1–1.7-mm *ESD*, were significantly correlated (Fig. 8). At low concentrations of LCs, such as in the integrated net tows in SP05, the relationship is more variable. A similar relationship was reported for net- and LOPC-based estimates of *Calanus finmarchicus*, in which variability increased at lower concentrations (Heath et al. 1999). The LOPC-based estimate is sensitive to the *AI* and the size range used. We used $AI > 0.6$ to exclude transparent particles. The size

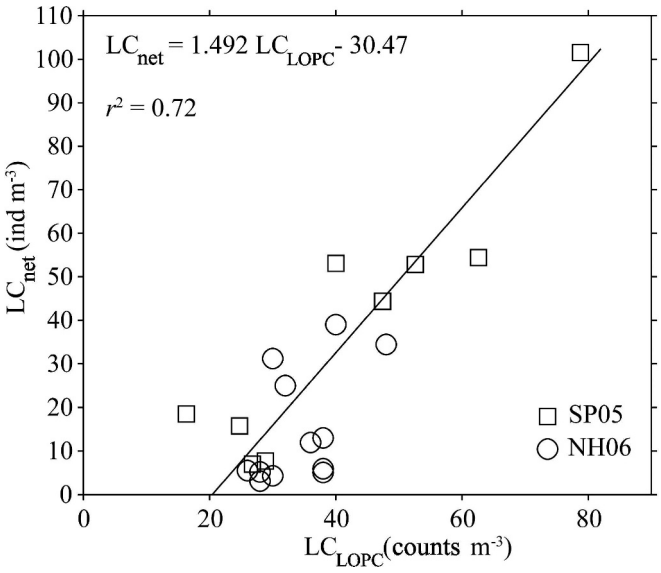

Fig. 8. Large copepod abundance (counts m^{-3}) estimated from net-LOPC MEP data in relation to abundance (individuals m^{-3}) estimated from microscopic analysis of net samples. Linear regression is shown.

range (1.1–1.7-mm *ESD*) was based on published values of *ESD* for LCs in this region (Osgood and Checkley 1997; Beaulieu et al. 1999) and the *ESD* estimated from microscopic measurements of the length and width of the cephalothorax of the LCs in our net samples. This size range is also consistent with variation in eigenvectors 1 and 2 for SP07 2 (Fig. 7). SOLOPC 2 was deployed at 17:38 h on 23 Apr 07. The first two profiles showed high abundances of particles characteristic of LCs; note the high initial values of total particle concentration (mL m^{-3}) in Fig. 4 for SOLOPC 2 in SP07. Two net tows showed that *C. pacificus* C5 and adults were abundant (summed abundances for these two net tows were 70 and 74 individuals m^{-3}, respectively) and dominated LCs by number (92, 98%) and volume (94, 98%). Eigenvector 1 (2) shows a maximum (minimum) at ~1.2-mm *ESD* (arrows, Fig. 7). We propose that these peaks (troughs) are due to abundant *C. pacificus* C5 and adults sensed by SOLOPC 2 early in its deployment. Eigenvector analysis of particle size spectra from LOPC data collected in waters dominated by discrete size classes of zooplankton may provide an objective means to estimate the *ESD* of discrete types of zooplankton. A second source of variability in this

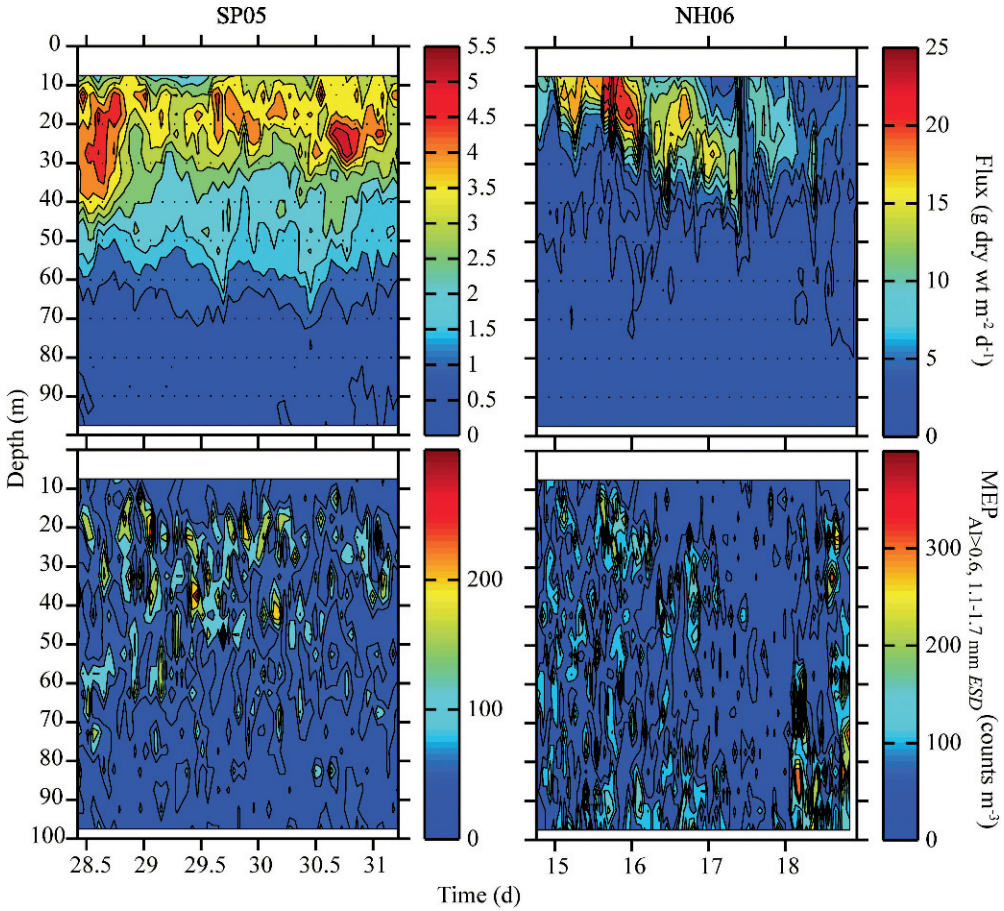

Fig. 9. Estimated particle flux (upper panels) and abundance of MEPs the size (*ESD* 1.1–1.7 mm) and transparency ($AI > 0.6$) of large copepods (lower panels) for SP05 (2005) and NH06 (2006).

Table 1. Correlations (r) of integrated particulate volume (Integ. part. vol.) and score of first eigenvector (EV1) with Chl *a* fluorescence. Each r is significant at $p < 0.001$.*

Cruise	SOLOPC	n	r, Integ. part. vol.	r, EV1
Sproul 2005	1	n/a	n/a	n/a
New Horizon 2006	1	1621	0.52	0.01
Sproul 2007	1	171	0.71	0.44
Sproul 2007	2	228	0.39	−0.06

* n/a, SOLOPC did not have a fluorometer during Sproul 2005.

relationship (Fig. 8) is the fraction of total particles of types other that LCs, increasing as LCs become scarce (e.g., $<\sim$50 individuals m^{-3}). The positive X-intercept of the linear regression for this relationship indicates particles were sensed by the LOPC that were not collected by the net and were counted microscopically as LCs. Such particles may have been collected by the net but were not LCs and/or have been fragile and have not been retained by the net (cf., González-Quirós and Checkley 2006); we believe the former less likely than the latter, as most particles, including plankton, in the size range of 1.1–1.7-mm *ESD* were LCs, based on visual inspection of our samples.

Property distributions—We hypothesized that many of the particles sensed by the SOLOPC, and much of their volume, are aggregates formed from the products of photosynthesis, including phytoplankton, fecal pellets, and other detritus, and lost by grazing and sinking. The following results are consistent with this hypothesis.

Most or all of the water column sampled in each deployment was stratified, with shallow mixed layers in SP05 and NH06. Chl *a* fluorescence was maximal in the pycnocline either immediately beneath the base of the mixed layer (SP05) or near surface (NH06). The maximal concentration of all particles, by number and volume, was associated with the Chl *a* maximum in each of the four deployments (Fig. 4). Total particulate volume was correlated with Chl *a* fluorescence (Table 1). In two of the three SOLOPC deployments with a fluorometer, the score of the first eigenvector was not correlated with Chl *a* fluorescence; in the third, it was correlated, but more weakly than was the total particulate volume. This indicates that many of the sensed particles were derived from the phytoplankton (e.g. through the aggregation of phytoplankters, fecal pellets, or detritus derived from the phytoplankton) and that the larger particles, characterized by eigenvectors 1 and 2, did not co-occur with the phytoplankton.

When collected into four time-of-day averages, the normalized volume spectra show a concentration maximum between 10 and 20 m, the strength of which changes through the day (Fig. 5). The nVd is greatest for particles 600–800 μm in *ESD* in the late afternoon–early evening; the nVd maximum is smallest in the early morning. The size of the particles shifts to larger particles with increasing depth.

The transparency of MEPs ranged broadly. At one extreme, there were many transparent particles, some with *OD* as large as 1.5 cm, and most with *ESD* of $<\sim$1 mm (Fig. 6). Such particles may be marine snow and may include aggregates, larvacean houses, and gelatinous zooplankters. At the other end of this range were fewer, relatively opaque particles. We suggest that these include crustacean zooplankton, especially copepods ($\sim$1–2-mm *ESD*) and euphausiids ($\sim$2–6-mm *ESD*).

The eigenvectors tend to describe variations in one sharply defined size category. Such a pattern is to be expected if the animals of similar sizes dominate the variability (e.g., Herman et al. 2004, and references therein). It contrasts with the broad shape of the average nVd spectrum, which is similar to that described for marine snow particles in Monterey Bay (Jackson et al. 1997).

Collectively, our results are consistent with a conceptual model of daytime production of the phytoplankton and perhaps their extracellular products (e.g., transparent exopolymer particles; Passow 2002), followed by aggregation of phytoplankton, feces, and other detritus, and loss of aggregates by sinking and grazing. Such a model is consistent with observations of diel variation in the concentration of aggregates below the euphotic zone at 270 m (Lampitt et al. 1993) and in the surface waters of the Santa Barbara Channel (Graham et al. 2000). It was recently reported (L. Abramson unpubl.) that pigment biomarkers in particles suspended at 200 m, beneath the euphotic zone, are more similar to those in phytoplankton and particles suspended at 20 m than particles collected in sediment traps at 200 m, implying rapid transport to depth followed by disaggregation. Eppley et al. (1977) showed that particulate organic matter suspended in the euphotic zone off Southern California was either living phytoplankton or recently derived from it. Ruiz (1997) modeled diel variation in the concentration of marine snow and concluded that diel variation in turbulence in the mixed layer was the most likely cause. Thus, our results from use of the SOLOPC, together with the literature, are consistent with a conceptual model of daytime primary production, aggregation, sinking out of the euphotic zone, and, perhaps, disaggregation below.

The patterns of estimated particle flux and large copepods (Fig. 9) indicate the possible grazing by LCs on sinking particles. Dagg (1993) concluded that *Neocalanus cristatus* in the subarctic Pacific Ocean feed primarily on aggregates sinking out of the euphotic zone. Large copepods, including *C. pacificus* and *M. lucens*, have been observed to occur beneath the depth of maximal phytoplankton abundance in Dabob Bay, Washington (Dagg et al. 1998). An alternative to grazing on sinking particles is brief forays into the region of high particle abundance (Pearre 2003).

In conclusion, the SOLOPC is an autonomous, Lagrangian profiling SOLO float with LOPC and ECO Puck fluorometer. It assesses the distribution and abundance of plankton and other particles 100 μm–1-cm *ESD* and their ambient environment in the upper 300 m, with a resolution of a meter in the vertical and as little as an hour or less in time. Its lack of attachment to a surface vessel may be advantageous in minimizing disruption of fragile particles and avoidance by zooplankton. Challenges include bio-

fouling during long deployments and inference about distinct types of plankton and other particles.

In the future, the SOLOPC may be recovered, as described here, or not. In both modes, ancillary information from other ALPS, ships, and satellites will valuably complement the information obtained from the SOLOPC. Of particular value is the collection of zooplankton near the SOLOPC to facilitate inference about the zooplankton from the LOPC data. We believe that both microscopic analysis of net samples and eigenvector analysis of LOPC size spectra will be particularly valuable in this regard. We anticipate that the SOLOPC will be useful in studies of phytoplankton, primary production, zooplankton, grazing, other particles, and sinking flux. The current cost to produce a SOLOPC is approximately equivalent to the cost of using an ocean-class research ship for ~1.5 d. In this context, the value of the SOLOPC to assess plankton and other particles remotely and autonomously over weeks to months or longer is apparent. A broadly distributed deployment of SOLOPCs within the large, existing array of ARGO floats has the potential to provide insight into the biological pump, and thus the ocean carbon cycle, and phenological changes in plankton dynamics, particularly in the context of global change.

Finally, we emphasize the importance of observing plankton and other particles in situ in a Lagrangian frame of reference. The use of meshes, including fine filters and coarser nets, remains the conventional means to observe the plankton and other particles. While necessary, such devices filter our view of the natural world (cf., Haury et al. 1978) and thus our understanding of it. We believe that in situ observation with a diverse array of autonomous, Lagrangian sensors and platforms is useful, if not necessary, to achieve an understanding of pelagic ecology and biogeochemistry.

References

Alldredge, A. L., and C. Gotschalk. 1988. In situ settling behavior of marine snow. Limnol. Oceanogr. **33:** 339–351.

Baumgartner, M. F. 2003. Comparisons of *Calanus finmarchicus* fifth copepodite abundance estimates from nets and an optical plankton counter. J. Plankton Res. **25:** 855–868.

Beaulieu, S. E., M. M. Mullin, V. T. Tang, S. M. Pyne, A. L. King, and B. S. Twining. 1999. Using an optical plankton counter to determine the size distributions of preserved zooplankton samples. J. Plankton Res. **21:** 1939–1956.

Bograd, S. J., D. M. Checkley Jr., and W. S. Wooster. 2003. CalCOFI: A half century of physical, chemical, and biological research in the California Current System. Deep-Sea Res. II **50:** 2349–2353.

Dagg, M. 1993. Sinking particles as a possible source of nutrition for the large calanoid copepod *Neocalanus cristatus* in the subarctic Pacific Ocean. Deep-Sea Res. I **40:** 1431–1445.

———, B. W. Frost, and J. Newton. 1998. Diel vertical migration and feeding in adult female *Calanus pacificus*, *Metridia lucens* and *Pseudocalanus newmani* during a spring bloom in Dabob Bay, a fjord in Washington USA. J. Mar. Sys. **15:** 503–509.

Davis, C. S., S. M. Gallagher, M. S. Berman, L. R. Haury, and J. R. Strickler. 1992. The Video Plankton Recorder (VPR): Design and initial results. Arch. Hydrobiol. Beih. **36:** 68–71.

Davis, R. E., J. T. Sherman, and J. Dufour. 2001. Profiling ALACEs and other advances in autonomous subsurface floats. J. Atmos. Oceanic Tech. **18:** 982–993.

———, D. C. Webb, L. A. Regier, and J. Dufour. 1992. The Autonomous Lagrangian Circulation Explorer (ALACE). J. Atmos. Oceanic Tech. **9:** 264–285.

Dever, E. P. 1997. Wind-forced cross-shelf circulation on the northern California shelf. J. Phys. Oceanogr. **27:** 1566–1580.

Emery, W. J., and R. E. Thomson. 1997. Data analysis methods in physical oceanography. Pergamon.

Eppley, R. W. [ed.]. 1986. Plankton dynamics of the Southern California Bight. Springer.

———, W. G. Harrison, S. W. Chisholm, and E. Stewart. 1977. Particulate organic matter in surface waters off southern California and its relationship to phytoplankton. J. Mar. Res. **35:** 671–696.

González-Quirós, R., and D. M. Checkley, Jr. 2006. Occurrence of fragile particles inferred from optical plankton counters used in situ and to analyze net samples collected simultaneously. J. Geophys. Res. **111:** C05S06, doi:10.1029/2005JC003084.

Gorsky, G., M. Picheral, and L. Stemmann. 2000. Use of the Underwater Video Profiler for the study of aggregate dynamics in the North Mediterranean. Estuar. Coast. Shelf Sci. **50:** 121–128.

Graham, W. M., S. MacIntyre, and A. L. Alldredge. 2000. Diel variations of marine snow concentration in surface waters and implications for particle flux in the sea. Deep-Sea Res. I. **47:** 367–395.

Haury, L. R., J. A. McGowan, and P. H. Wiebe. 1978. Patterns and processes in the time-space scales of plankton distributions, p. 277–327. *In* J. H. Steele [ed.], Spatial pattern in plankton communities. Plenum. 277–327.

Heath, M. R., J. Dunn, J. G. Fraser, S. J. Hay, and H. Madden. 1999. Field calibration of the Optical Plankton Counter with respect to *Calanus finmarchicus*. Fish. Oceanogr. **8:** 13–24.

Herman, A. W. 1988. Simultaneous measurement of zooplankton and light attenuance with a new optical plankton counter. Cont. Shelf Res. **8:** 205–221.

———, B. Beanlands, and E. F. Phillips. 2004. The next generation of Optical Plankton Counter: The Laser-OPC. J. Plankton Res **26:** 1135–1145.

———, and M. Harvey. 2006. Application of normalized biomass size spectra to laser optical plankton counter net intercomparisons of zooplankton distributions. J. Geophys. Res. **111:** C05S05, doi:10.1029/2005JC002948.

Jackson, G. A., R. Maffione, D. K. Costello, A. L. Alldredge, B. E. Logan, and H. G. Dam. 1997. Particle size spectra between 1 μm and 1 cm at Monterey Bay determined using multiple instruments. Deep-Sea Res. I **44:** 1739–1767.

Lampitt, R. S., W. R. Hillier, and P. G. Challenor. 1993. Seasonal and diel variation in the open ocean concentration of marine snow aggregates. Nature **362:** 737–739.

Osgood, K. E., and D. M. Checkley, Jr. 1997. Observations of a deep aggregation of *Calanus pacificus* in the Santa Barbara Basin. Limnol. Oceanogr. **42:** 997–1001.

Passow, U. 2002. Transparent exopolymer particles (TEP) in aquatic environments. Prog. Oceanogr. **55:** 287–333.

Pearre, S. 2003. Eat and run? The hunger/satiation hypothesis in vertical migration: History, evidence and consequences. Biol. Rev. **78:** 1–79.

Preisendorfer, R. W. 1988. Principal component analysis in meteorology and oceanography. Elsevier

ROEMMICH, D., S. RISER, R. DAVIS, AND Y. DESAUBIES. 2004. Autonomous profiling floats: Workhorse for broad-scale ocean observations. Mar. Technol. Soc. J. **38:** 21–29.

RUIZ, J. 1997. What generates daily cycles of marine snow? Deep-Sea Res. I **44:** 1105–1126.

RYKACZEWSKI, R. R., AND D. M. CHECKLEY, JR. 2008. Influence of ocean winds on the pelagic ecosystem in upwelling regions. Proc. Natl. Acad. Sci. USA **105:** 1965–1970.

SAMSON, S., T. HOPKINS, A. REMSEN, L. LANGEBRAKE, T. SUTTON, AND J. PATTEN. 2001. A system for high-resolution zooplankton imaging. IEEE J. Ocean. Eng. **26:** 671–676.

Received: 2 October 2007
Accepted: 10 April 2008
Amended: 20 June 2008